The adaptor protein melanophilin regulates dynamic myosin-Va:cargo interaction and dendrite development in melanocytes

Christopher L. Robinson[a], Richard D. Evans[a], Kajana Sivarasa[a], Jose S. Ramalho[b], Deborah A. Briggs[a], and Alistair N. Hume[a,*]

[a]School of Life Sciences, University of Nottingham, Nottingham NG7 2UH, United Kingdom; [b]CEDOC Faculdade de Ciencias Medicas, Universidade Nova de Lisboa, 1169-056 Lisbon, Portugal

ABSTRACT **The regulation of organelle transport by the cytoskeleton is fundamental for eukaryotic survival. Cytoskeleton motors are typically modular proteins with conserved motor and diverse cargo-binding domains. Motor:cargo interactions are often indirect and mediated by adaptor proteins, for example, Rab GTPases. Rab27a, via effector melanophilin (Mlph), recruits myosin-Va (MyoVa) to melanosomes and thereby disperses them into melanocyte dendrites. To better understand how adaptors regulate motor:cargo interaction, we used single melanosome fluorescence recovery after photobleaching (smFRAP) to characterize the association kinetics among MyoVa, its adaptors, and melanosomes. We found that MyoVa and Mlph rapidly recovered after smFRAP, whereas Rab27a did not, indicating that MyoVa and Mlph dynamically associate with melanosomes and Rab27a does not. This suggests that dynamic Rab27a:effector interaction rather than Rab27a melanosome:cytosol cycling regulates MyoVa:melanosome association. Accordingly, a Mlph-Rab27a fusion protein reduced MyoVa smFRAP, indicating that it stabilized melanosomal MyoVa. Finally, we tested the functional importance of dynamic MyoVa:melanosome interaction. We found that whereas a MyoVa-Rab27a fusion protein dispersed melanosomes in MyoVa-deficient cells, dendrites were significantly less elongated than in wild-type cells. Given that dendrites are the prime sites of melanosome transfer from melanocytes to keratinocytes, we suggest that dynamic MyoVa:melanosome interaction is important for pigmentation in vivo.**

Monitoring Editor
Erika Holzbaur
University of Pennsylvania

Received: Apr 17, 2018
Revised: Jan 23, 2019
Accepted: Jan 25, 2019

INTRODUCTION

Organelle distribution and transport are fundamental for eukaryotic survival. Motor proteins of the kinesin, dynein, and myosin families are essential for organelle transport along microtubule (MT) and filamentous actin (F-actin) tracks, respectively (Hirokawa *et al.*, 2009; Kardon and Vale, 2009; Hartman *et al.*, 2011). In general, motor protein-heavy chains have a modular structure, and are composed of relatively conserved motor domains that bind to F-actin/MT tracks and generate force through hydrolysis of ATP, coupled to more diverse tails, that link the motor to cargo, for example, organelles (Hirokawa *et al.*, 2009; Kardon and Vale, 2009; Hartman *et al.*, 2011). In some cases, motor tails appear to contain lipid-binding domains; for example, kinesins, KIF1a and KIF1bβ, and type I myosins contain plekstrin homogy (PH) domains and thus may directly target organelle membranes via interaction with membrane lipids (Kardon and Vale, 2009; Hartman *et al.*, 2011). However, cargo attachment appears to be more frequently mediated by interaction of the motor tail with cargo-binding light chains that are often membrane-associated proteins. Among these, small GTPases of the Rab family are well represented (Hammer and Wu, 2002; Stenmark, 2009; Hutagalung and Novick, 2011).

This article was published online ahead of print in MBoC in Press (http://www.molbiolcell.org/cgi/doi/10.1091/mbc.E18-04-0237) on January 30, 2019.

*Address correspondence to: Alistair N. Hume (Alistair.hume@nottingham.ac.uk).

Abbreviations used: F-actin, filamentous actin; FCS, fetal calf serum; GDI, GDP dissociation inhibitor; GDP, guanosine diphosphate; GFP, enhanced green fluorescent protein; HMM, heavy meromyosin; HUVECs, human umbilical vein epithelium cells; Mlph, melanophilin; MT, microtubule; Myo-FL, full length myosin-Va; Myo-T, GFP fused with the melanocyte-specific tail of myosin-Va; MyoVa, myosin-Va; PBFI, prebleach fluorescence intensity; PH, plekstrin homogy; R27BD, Rab27-binding domain; smFRAP, single melanosome fluorescence recovery after photobleaching.

Rabs are the largest family of small Ras-like GTPases (>60 proteins in humans). In general, Rabs are thought to function as compartment-specific molecular switches that regulate transport through the endocytic and secretory pathways of eukaryotes (Stenmark, 2009; Hutagalung and Novick, 2011; Barr, 2013; Pfeffer, 2017). Rabs associate with organelles via interaction of geranylgeranyl isoprene moieties, which are covalently posttranslationally attached to C-terminus cysteines, with lipids of the cytoplasmic face of organelle membranes. There, active GTP-bound Rabs recruit a diverse group of effector proteins, for example, motor proteins, protein/lipid kinases, and membrane-tethering and docking factors from the cytosol that transduce their function(s) in transport. Rab activity is terminated by GTP hydrolysis-dependent destabilization of the conformation of the effector binding "switch regions." This reduces the Rab:effector interaction affinity resulting in the release of effectors from membranes. General models consider that inactive guanosine diphosphate (GDP)-bound Rabs are then extracted from membranes into the cytosol by Rab GDI (GDP dissociation inhibitor) and recycled for use in further rounds of transport. This suggests that the coupled GTP/GDP binding and membrane/cytosol cycles of Rab GTPases could control the transport function of motor proteins by regulating their association with cargo.

Type V myosins, such as myosin-Va (MyoVa), have highly conserved roles in organelle transport in eukaryotes, and a number of Rabs recruit them to cargo (Lindsay *et al.*, 2013). For example, in yeast, direct interaction of Myo2 with ypt31/32 (Rab11 in yeast), and ypt11, drives the polarized delivery of secretory vesicles and mitochondria, respectively, to the growing bud (Lipatova *et al.*, 2008; Chernyakov *et al.*, 2013). In mammalian neurones, myosin-Vb, one of three type V myosins, is recruited to recycling endosomes by Rab11 and its effector FIP2 and regulates AMPA receptor trafficking and dendritic spine growth that is important in memory and learning (Wang *et al.*, 2008).

MyoVa, like other type V motors, is composed of a dimer of motor-heavy chains, each of which consists of four domains: motor (head), lever arm, dimerization, and globular tail (Trybus, 2008; Hammer and Sellers, 2012). The motor is conserved among myosins and contains F-actin-binding and ATPase activities. ATP binding and hydrolysis regulate interaction with F-actin and generate a conformational change (or power-stroke) necessary for movement. The power-stroke is amplified by the long (24 nm) light chain/calmodulin-binding lever arm, resulting in the detachment and reattachment of the partner motor domain and displacement of the dimer toward the plus end of the track. Dimerization is achieved by α-helical coiled–coil interaction, and the tail and alternatively spliced region mediate cargo binding and regulation of motor activity through direct intramolecular (head–tail) interaction with the motor (Krementsov *et al.*, 2004; Li *et al.*, 2004; Wang *et al.*, 2004). A series of elegant in vitro studies using single molecule imaging, x-ray crystallography, electron microscopy, and rapid acquisition atomic force microscopy indicate that MyoVa is a processive motor undertaking multiple (10–100 s) catalytic cycles coupled to mechanical changes that move the motor along F-actin with 36-nm steps, corresponding to the helical repeat distance of the filament. These studies indicate that MyoVa moves at 250–450 nm/s in a hand-over-hand manner with each head alternating in the lead or trailing position (Hammer and Sellers, 2012).

In melanocytes, an alternatively spliced MyoVa isoform plays an essential role in transporting pigment-filled melanosomes into a peripheral network of cell extensions, termed dendrites, which may contact up to 40 keratinocytes. From there, melanosomes are transferred to adjacent keratinocytes. This process is fundamental for pigmentation of skin and hair in mammals (Van Den Bossche *et al.*, 2006; Wu and Hammer, 2014). Consistent with this, a deficiency of MyoVa results in defects in the melanosome transport within melanocytes and their transfer to keratinocytes (Van Gele *et al.*, 2009). Recruitment of MyoVa to melanosomes is dependent on Rab27a and its effector melanophilin (Mlph) (Fukuda *et al.*, 2002; Nagashima *et al.*, 2002; Strom *et al.*, 2002; Wu *et al.*, 2002b). Melanocyte-spliced MyoVa contains exon F in the C-terminus portion of the dimerization domain that allows Mlph to recruit it to melanosomes (Wu *et al.*, 2002a). Mlph has a modular structure composed of 1) an N-terminus Rab27-binding domain (R27BD) that is conserved among most Rab27 effector proteins, and 2) a C-terminus MyoVa and F-actin-binding domains that are conserved with myosin-VIIa Rab-interacting protein, but not other Rab27 effectors (Kuroda *et al.*, 2003; Hume *et al.*, 2006; Fukuda, 2013). Thus, Mlph plays a vital role in allowing Rab27a to recruit MyoVa to melanosomes indirectly. However, given that models of Rab function predict that the GTPase activity and hypothetical membrane/cytosol cycling activity of Rab27a could regulate motor:cargo attachment, the basis of the requirement for Mlph in MyoVa recruitment, beyond providing a binding site for melanocyte-spliced MyoVa, is unclear.

In this study, we used single melanosome fluorescence recovery after photobleaching (smFRAP) to directly examine the kinetics of the interaction between MyoVa and a model cargo; the melanosome in melanocytes. We found that MyoVa and Mlph dynamically associate with melanosomes, whereas Rab27a was less dynamic. Using a Mlph-Rab27a fusion protein (Mlph-Rab), we show that dynamic Rab27a:Mlph interaction in part regulates myosin:melanosome interaction. Finally, using a MyoVa-Rab27a fusion protein (Myo-Rab), we show that recycling of MyoVa during melanosome transport is important for the elongated shape of melanocytes. These data highlight a novel and unexpected aspect of Mlph function in regulating the kinetics of MyoVa–organelle interaction and indicate that the dynamics of cargo:cytoskeleton interactions can influence cell structure and transport at the level of organelle populations.

RESULTS

smFRAP indicates rapid turnover of melanosome-associated MyoVa

To investigate the mechanism of MyoVa-dependent organelle transport and the role of adaptors in regulating the motor:cargo association, we used smFRAP to characterize the interaction between MyoVa and melanosomes in melanocytes. To do this, we transiently expressed an enhanced green fluorescent protein (GFP)-tagged version of the melanosome-binding myosin-Va tail (Myo-T) in wild-type melanocytes (melan-a) (Figure 1A). We then used confocal microscopy to record the distribution and dynamics of Myo-T and melanosomes and their interaction in living melanocytes. Consistent with previous studies, we found that puncta of Myo-T associated with pigmented melanosomes (Figure 1B, arrows) (Wu *et al.*, 1998; Hume *et al.*, 2001).

We then photobleached Myo-T fluorescence associated with well-separated melanosomes and recorded the subsequent recovery of fluorescence on individual organelles (Figure 1). We observed rapid, partial recovery of melanosomal Myo-T fluorescence after photobleaching (Figure 1, B and C; Supplemental Movie 1; mean $t_{1/2}$ of recovery [s] = 33.12 ± 10.09; mean recovery plateau [% prebleach fluorescence intensity] PBFI = 67.86 ± 8.775; mean maximum recovery [%PBFI] 82.29 ± 14.05). These data suggest that MyoVa dynamically associates with melanosomes. Similar results were obtained from studies using Myo-T and full-length myosin-Va (Myo-FL) transiently expressed in MyoVa-deficient (melan-d) cells (the latter at rescuing, i.e., functionally relevant levels) (Supplemental Figure S1 and Supplemental Movies 2 and 3; mean $t_{1/2}$ rec [s] = 24.69 ± 12.6 [Myo-T], 14.11 ± 6.626 [Myo-FL]; mean recovery

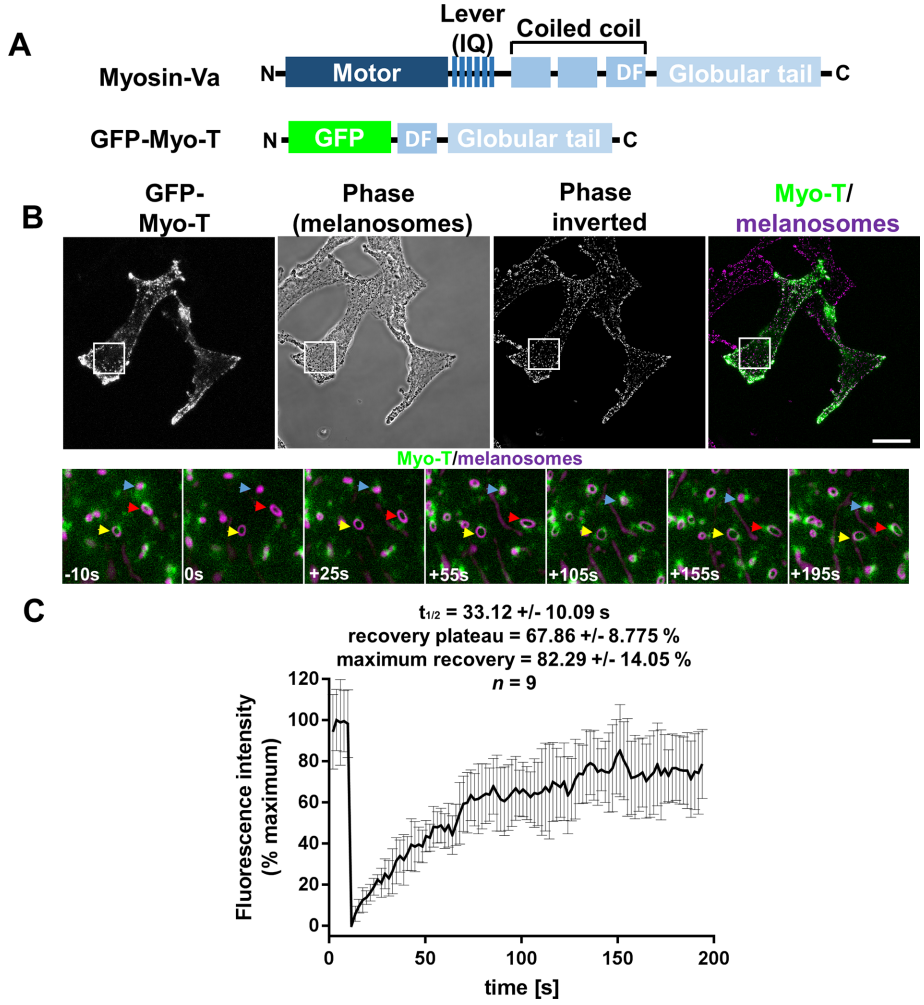

FIGURE 1: smFRAP analysis of the turnover of melanosome-associated Myo-T in melanocytes. Wild-type (melan-a) cells were cultured in glass-bottomed dishes, transfected with a Myo-T expression vector, and the dynamics of the association of Myo-T with melanosomes were investigated using smFRAP analysis (see *Materials and Methods*). (A) Schematic representation of the structure of experimental proteins. D and F indicate the position of the Mlph-interacting motif encoded by alternatively spliced exons. (B) (Top panels) Example images showing the distribution of Myo-T and melanosomes and their coincidence in living cells. Scale bar = 20 μm. White boxes indicate the parts of cells that were subjected to smFRAP analysis and are shown in the high-magnification images below. (Bottom panels) Images taken from example smFRAP series captured at the indicated time relative to photobleaching ($t = 0$). Colored arrows in these images highlight the position of single melanosomes that were selectively photobleached over time (see Supplemental Movie 1). (C) Line plot showing the average fluorescence intensity associated with photobleached melanosomes over time. Error bars are SD; $n = 9$ melanosomes analyzed.

plateau [%PBFI] = 33.85 ± 15.69 [Myo-T], 38.8 ± 21.91 [Myo-FL]; mean maximum recovery [%PBFI] = 44.48 ± 22.89 [Myo-T], 53.63 ± 14.82 [Myo-FL]). One possible explanation for higher recovery of Myo-T in melan-a versus melan-d cells is that interaction with endogenous MyoVa enhances the level of recovery in melan-a cells.

Rab27a stably associates with melanosomes in melanocytes

To probe the role of cargo adaptors in regulating the turnover of MyoVa, we investigated the kinetics of the association of Rab27a with melanosomes. GTP-bound/active Rab27a was previously shown to recruit MyoVa to melanosomes via its effector Mlph (Hume and Seabra, 2011; Hammer and Sellers, 2012; Fukuda, 2013). As outlined above, Rab GTPases are proposed to couple cycles of GTP hydrolysis/GDP-GTP exchange with membrane association and disassociation, thus regulating the association of their effectors, for example, Mlph/MyoVa, with membranes (Stenmark, 2009; Hutagalung and Novick, 2011). Therefore, we hypothesized that the dynamic interaction of MyoVa with the melanosome membrane might be due to a similarly dynamic Rab27a:melanosome interaction. To test this, we transiently expressed GFP-Rab27a in wild-type (melan-a) and Rab27a null (melan-ash) melanocytes. As previously reported, we observed that GFP-Rab27a codistributed with melanosomes in melanocytes and restored peripheral melanosome distribution in Rab27a-deficient cells confirming the functionality of GFP-Rab27a (Figure 2, A and B) (Bahadoran *et al.*, 2001; Hume *et al.*, 2001; Wu *et al.*, 2001).

Using smFRAP analysis in both cell types, we observed significantly lower levels of recovery of GFP-Rab27a to individual melanosomes compared with Myo-T expressed in wild-type melan-a, suggesting that Rab27a more stably associates with melanosomes compared with MyoVa (Figure 2, A, B, and E; Supplemental Movies 4 and 5). The low level of Rab27a recovery in smFRAP experiments prevented reliable modeling of the data to a single exponential function and determination of the half-time and plateau of recovery. Therefore, we report only mean maximum recovery (%PBFI) for each population as a measure of FRAP in these experiments (melan-a = 13.42 ± 4.27 and melan-ash = 26.44 ± 10.65; Supplemental Figure S2A).

To investigate whether interaction with effectors stabilizes melanosomal Rab27a, we tested the recovery of 1) GFP-Rab27a in Mlph-deficient cells (melan-ln) and 2) effector interaction-deficient melanosome-targeted mutant GFP-Rab27a^{SF1F4} in wild-type (melan-a) cells (Tarafder *et al.*, 2011). Consistent with the other smFRAP experiments using GFP-Rab27a (Figure 2, A and B), we observed levels of fluorescence recovery that were significantly lower compared with Myo-T (Figures 1, B and C, and 2, C–E; Supplemental Figure S2A, and Supplemental Movies 6 and 7; mean maximum recovery [%PBFI] = 17.11 ± 9.746% and 20.55 ± 9.484% for GFP-Rab27a in melan-ln and the GFP-Rab27a^{SF1F4} mutant in melan-a). This indicates that effectors do not significantly stabilize melanosomal Rab27a, that Rab27a more stably associates with melanosomes than MyoVa, and that dynamic interaction between MyoVa and melanosomes is not controlled directly by turnover of melanosomal Rab27a.

Mlph dynamically associates with melanosomes in melanocytes

As indicated above, Mlph directly interacts with MyoVa and Rab27a, thus allowing attachment of MyoVa to melanosomes (Fukuda *et al.*, 2002; Strom *et al.*, 2002; Wu *et al.*, 2002b). Dynamic interaction of Mlph with either (or both) of these partners could therefore provide

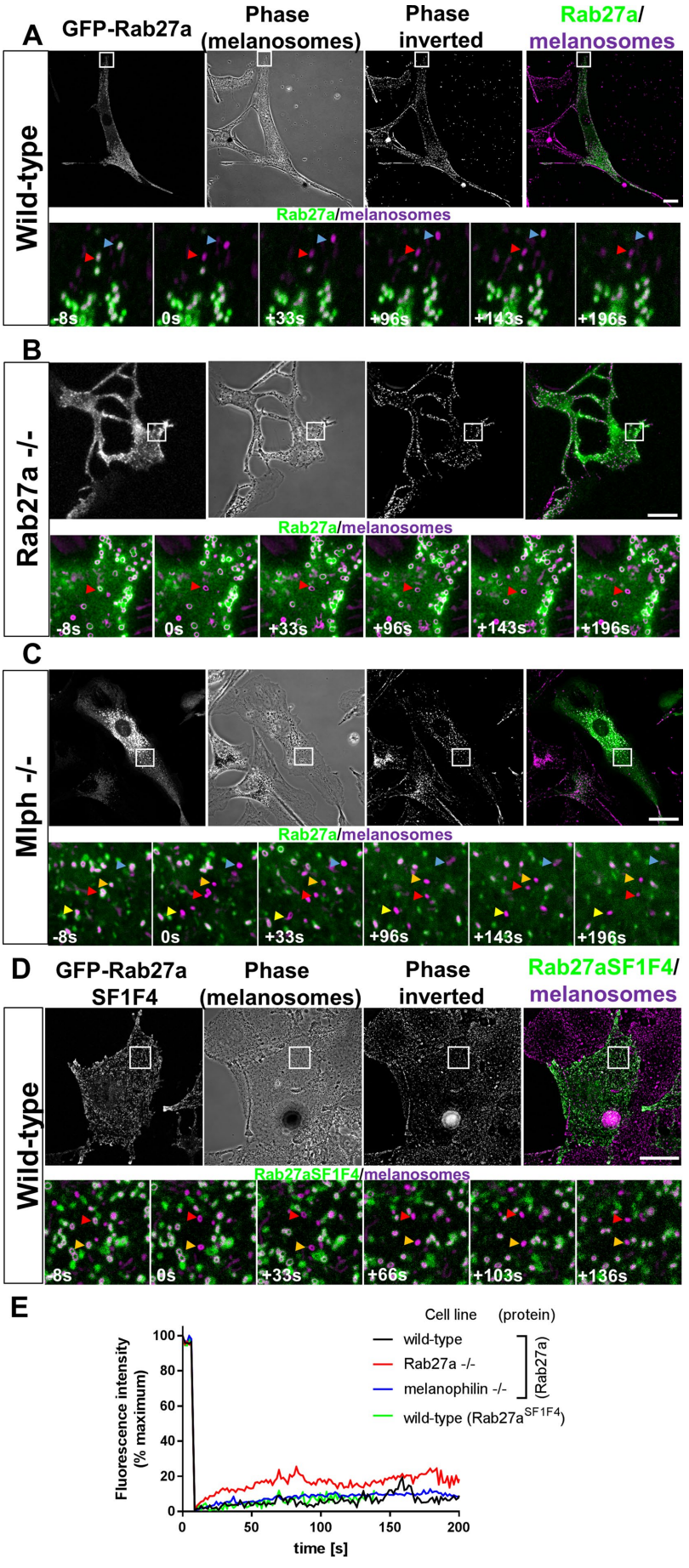

the basis of MyoVa turnover at the melanosome membrane. To examine this further, we used confocal microscopy to investigate the association between Mlph and melanosomes in living melanocytes. In line with the results of previous studies, we found that in wild-type (melan-a), Mlph null (melan-ln), and MyoVa null (melan-d) cells, transiently expressed GFP-Mlph was distributed throughout the cytoplasm and was enriched in puncta adjacent to melanosomes seen by phase contrast (Figure 3, A–C, red arrows in high-magnification images). This confirms that GFP-Mlph associates with melanosomes in a MyoVa-independent manner (Wu *et al.*, 2002b).

smFRAP experiments in wild-type (melan-a) cells showed that GFP-Mlph, like Myo-T, but not Rab27a, rapidly recovered on bleached melanosomes (Figures 1 and 3, A and D; Supplemental Figure S2 and Supplemental Movie 8; mean $t_{1/2}$ of recovery [s] = 12.67 ± 11.46; mean recovery plateau [%PBFI] = 73.2 ± 14.31; mean maximum recovery [%PBFI] = 82.26 ± 13.69). Similar results were seen in smFRAP studies of GFP-Mlph in Mlph null (melan-ln) and myosin-Va null (melan-d) cells (Figure 3, B–D; Supplemental Figure S2 and Supplemental Movies 9 and 10; mean $t_{1/2}$ of recovery [s] = 6.076 ± 3.369 and 5.396 ± 2.895; and mean recovery plateau [%PBFI] = 70.3 ± 10.13 and 65.25 ± 4.525; mean maximum recovery [%PBFI] = 98.88 ± 12.72 and 86.69 ± 14.65). Importantly, smFRAP studies of Mlph in Mlph null (melan-ln) cells were performed in cells in which GFP-Mlph rescued melanosome clustering, indicating that these experiments investigated the activity of functionally relevant levels of GFP-Mlph. In summary, these data indicate that Mlph, like MyoVa, turns over more rapidly than Rab27a at the melanosome membrane and suggest that Mlph interacts dynamically with Rab27a.

Dynamic Mlph:Rab27a interaction is a dominant factor regulating the MyoVa:melanosome association

Thus far, our data suggest that dynamic MyoVa:melanosome association may be regulated by

FIGURE 2: smFRAP analysis of the turnover of melanosome-associated Rab27a in melanocytes. Melanocytes were cultured in glass-bottomed dishes, transfected with GFP-Rab27a (A–C) (or GFP-Rab27a^{SF1F4} [D]) expression vectors, and the dynamics of the association of GFP-Rab27a with melanosomes were investigated using confocal FRAP analysis (see *Materials and Methods*). (A–D) (Top panels) Example images showing the distribution of GFP fusion protein and melanosomes in living wild-type (melan-a) (A and D), Rab27a –/– (melan-ash) (B), and Mlph –/– (melan-ln) (C) cells, respectively. White boxes indicate the parts of cells that were subjected to FRAP analysis and are shown in the high-magnification images below. Scale bars = 20 µm. Bottom panels are high-magnification images taken from example FRAP series captured at the indicated time relative to photobleaching ($t = 0$). Colored arrows highlight the position over time of melanosomes that were selectively photobleached. (E) Line plot showing the average fluorescence intensity associated with photobleached melanosomes over time; $n = 6$ (A), 7 (B), 6 (C), and 16 (D) melanosomes analyzed, respectively.

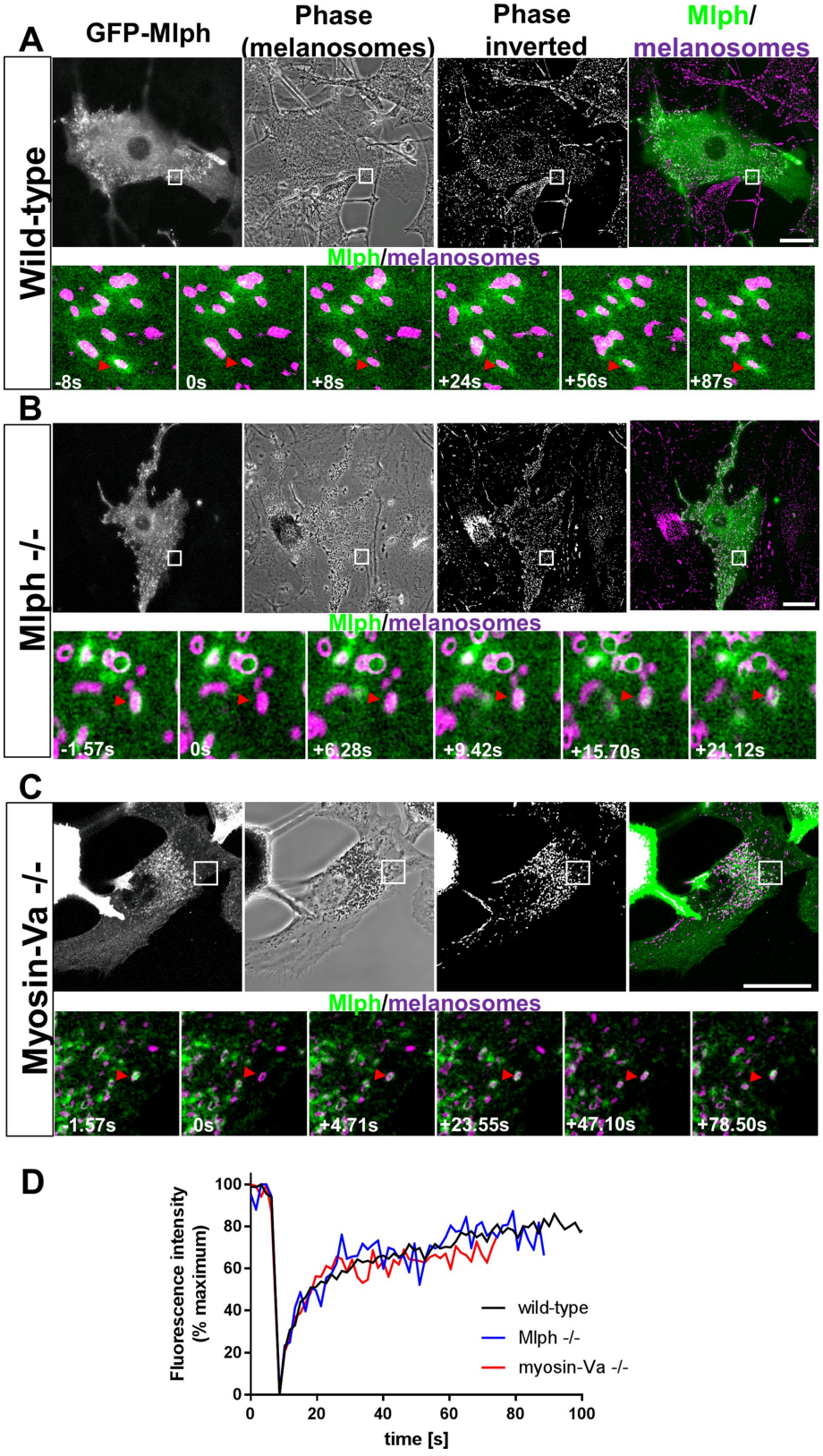

FIGURE 3: smFRAP analysis of the turnover of melanosome-associated Mlph in melanocytes. Melanocytes were cultured in glass-bottomed dishes, transfected with a vector expressing GFP-Mlph, and the dynamics of the association of GFP-Mlph with melanosomes were investigated using confocal FRAP analysis (see *Materials and Methods*). (A–C) Top panels are example images showing the distribution of GFP-Mlph and melanosomes in living wild-type (melan-a) (A), Mlph –/– (melan-ln) (B), and myosin-Va –/– (melan-d) (C) cells, respectively. Bottom panels are high-magnification images taken from example FRAP series captured at the indicated time relative to photobleaching ($t = 0$). Red arrows highlight the position over time of melanosomes that were selectively photobleached. White boxes in the top panels indicate the parts of cells that were subjected to FRAP analysis and are shown in the high-magnification images below. Scale bars = 20 μm. (D) Line plot showing the fluorescence intensity associated with photobleached melanosomes over time; $n = 10$ (A), 5 (B), and 5 (C) melanosomes analyzed, respectively.

dynamic Rab27a:Mlph and/or Mlph:MyoVa interaction. Consistent with this possibility, the overall profile of recovery after bleaching for Mlph and Myo-T in wild-type (melan-a) cells were more similar to one another than to Rab27a (Figures 1–3; Supplemental Figure S2). To investigate this further, we generated a vector allowing expression of an mCherry-tagged Mlph-Rab27a chimera that contains the C-terminus MyoVa and F-actin-binding domains (but not the N-terminus Rab27a-binding domain) of Mlph fused at the N-terminus of the Rab27a^{SF1F4} mutant (Figure 4A). As confirmed above, this mutant targets efficiently to melanosomes but does not interact with effectors (Figure 2D) (Tarafder *et al.*, 2011). Thus, it can be used to target proteins that are fused to it to melanosomes. We then coexpressed Mlph-Rab27a with Myo-T in Mlph –/– (melan-ln) melanocytes and used smFRAP to measure the dynamics of Myo-T:melanosome interaction. Parallel smFRAP experiments were carried out using mCherry alone and mCherry-Mlph.

In line with previous studies, we observed that mCherry-Mlph and mCherry-Mlph-Rab27a, but not mCherry alone, distributed in a punctate cytoplasmic pattern and that these puncta often colocalized with pigmented melanosomes, indicating that both proteins targeted to melanosomes (Figure 4B; Supplemental Figure S3, A and B). We also saw that expression of mCherry-Mlph and mCherry-Mlph-Rab27a rescued perinuclear melanosome clustering in Mlph –/– (melan-ln) cells in the majority of expressing cells, confirming that they were expressed at functionally relevant levels (Figure 4, B and C; Supplemental Figure S3D; mean pigment area [% total]; mCherry = 22.96 ± 6.855, mCherry-Mlph = 41.62 ± 30.98, mCherry-Mlph-Rab27a = 83.05 ± 13.13). Consistent with previous reports showing that high levels of Mlph expression disrupt melanosome dispersion, due to mistargeting of Mlph to peripheral F-actin, the

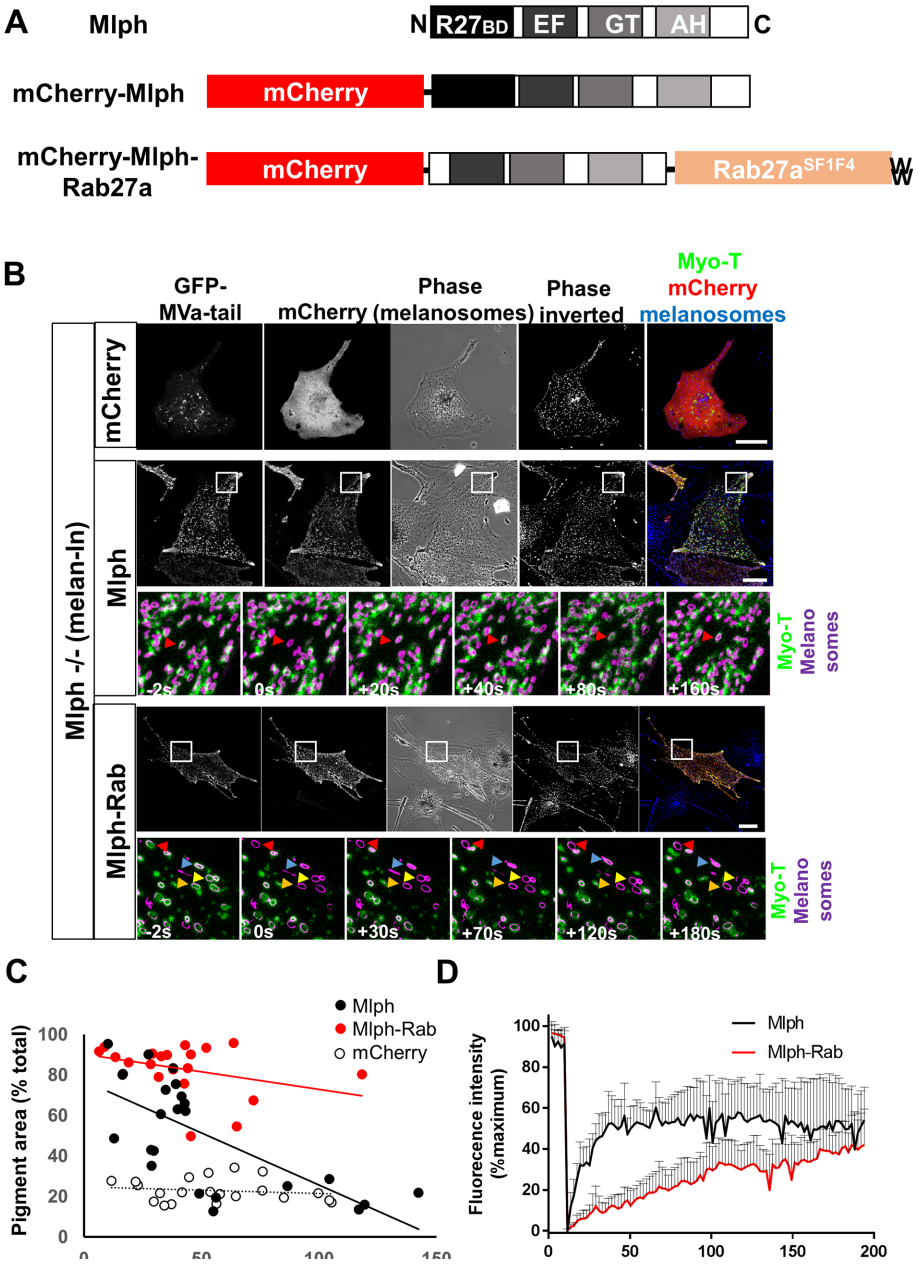

FIGURE 4: smFRAP analysis of the turnover of melanosome-associated Myo-T in melan-ln melanocytes coexpressing Mlph or Mlph-Rab27a. Mlph –/– (melan-ln) melanocytes were cultured in glass-bottomed dishes; transfected with vectors allowing expression of GFP-Myo-T in combination with mCherry alone (B), mCherry-Mlph (C), or mCherry-Mlph-Rab27a (D); and the dynamics of association of Myo-T with melanosomes were investigated using confocal FRAP analysis (see *Materials and Methods*). (A) Schematic representation of the structure of experimental proteins. R27BD, Rab27-binding domain; GT EF, MyoVa globular tail and exon F-binding domains; AH, amphipathic helix/actin-binding domain. (B) Top panels of each protein group are example images showing the distribution (or codistribution) of GFP-MyoVa-tail, mCherry, and melanosomes in living Mlph –/– cells prior to FRAP studies. Bottom panels (Mlph and Mlph-Rab groups) are high-magnification images taken from example FRAP series captured at the indicated time relative to photobleaching ($t = 0$). Colored arrows highlight the position over time of melanosomes that were selectively photobleached. White boxes in the top panels indicate the parts of cells that were subjected to FRAP analysis and are shown in the high-magnification images below (and inset in Supplemental Figure S3). Scale bars = 20 µm. (C) Scatter plot showing the relationship between expression level and functional efficiency of mCherry-Mlph and mCherry-Mlph-Rab27a, as reported by mean cellular fluorescence intensity (AU) and pigment area (% total cell area). Lines of best fit are shown in red (Mlph-Rab), black (Mlph), and dotted (mCherry). (D) Line plot showing the fluorescence intensity associated with photobleached melanosomes over time. The vertical bars above each plot indicate the SD. $n = 9$ (Mlph) and 7 (Mlph-Rab) melanosomes analyzed, respectively.

efficiency of rescue by mCherry-Mlph (but not mCherry-Mlph-Rab27a) correlated inversely with the protein expression level (Figure 4C; linear regression gradient and correlation coefficient R^2, mCherry = –0.0326 and 0.025, mCherry-Mlph = –0.1736 and 0.1193, and mCherry-Mlph-Rab27a = –0.5156 and 0.4849) (Hume *et al.*, 2006). Finally, we observed that Myo-T distributed in a melanosome-associated punctate pattern when coexpressed with Mlph-containing fusion proteins, but not mCherry alone, further confirming that both proteins are competent in recruiting MyoVa to melanosomes, (Figure 4B; Supplemental Figure S3, A and B).

smFRAP revealed that, when recruited to melanosomes by mCherry-Mlph, Myo-T turned over at a similar rate and extent to that seen for GFP-Mlph and Myo-T alone in wild-type (melan-a) cells (Figures 1, 3, and 4, B and D; Supplemental Figure S2 and Supplemental Movie 11; mean $t_{1/2}$ of recovery [s] = 16.81 ± 13.01, mean recovery plateau [%PBFI] = 58.17 ± 15.69%PBFI, and mean maximum recovery [%PBFI] = 73.76 ± 18.44). In contrast, when recruited by Mlph-Rab27a, although Myo-T recovered to a greater extent than Rab27a, it did so with slower kinetics and to a lesser extent than when recruited by Mlph (Figure 4, B and D; Supplemental Figure S2 and Supplemental Movie 12). Similar to Rab27a, several fluorescence recovery profiles for Myo-T coexpressed with Mlph-Rab27a could not be modeled using a single exponential function (Supplemental Figure S2; mean $t_{1/2}$ of recovery [s] = 61.02 ± 24.93, mean recovery plateau [%PBFI] = 42.77 ± 15.39, and mean maximum recovery [%PBFI] = 46.81 ± 15.36). smFRAP analysis of the Mlph-Rab27a fusion protein itself (tagged with GFP, i.e., GFP-Mlph-Rab27a) revealed that it recovered to a similar extent (no significant difference) to Myo-T coexpressed with Mlph-Rab27a (Supplemental Figures S4 and S2 and Supplemental Movie 13; mean $t_{1/2}$ of recovery [s] = 46.37 ± 23.33, mean recovery plateau [%PBFI] = 35.31 ± 18.39, and mean maximum recovery [%PBFI] = 39.63 ± 17.26). These observations indicate that the dynamic Mlph:Rab27a interaction may be the dominant factor regulating MyoVa turnover at the melanosome membrane.

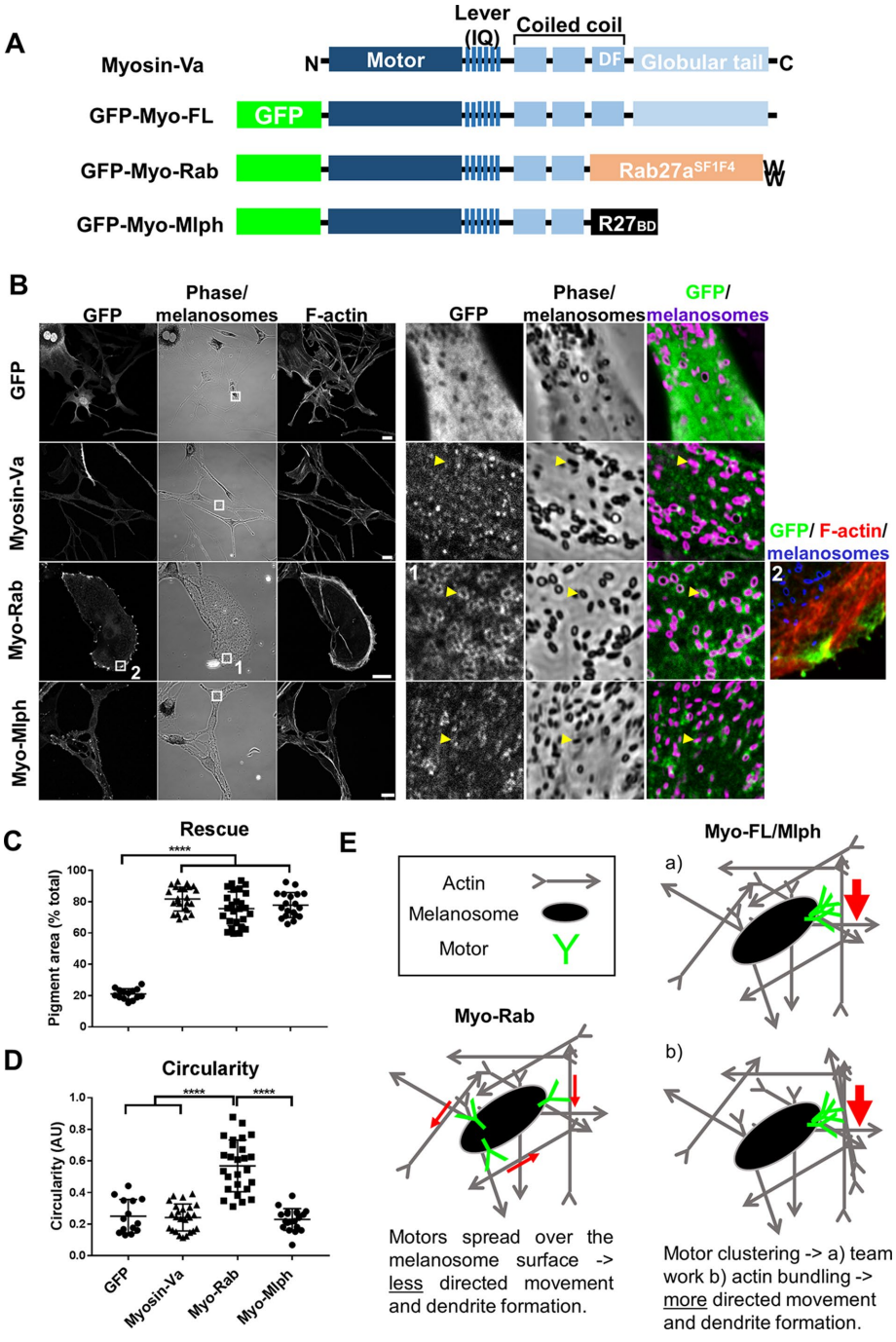

FIGURE 5: Fusion of active MyoVa with melanosome-associated Rab27a^{SF1F4} reduces its functional efficiency and affects dendrite development. Myosin-Va –/– (melan-d) cells were infected with adenoviruses expressing the indicated GFP fusion proteins, fixed and stained for immunofluorescence (see *Materials and Methods*). (A) Schematic representation of the structure of experimental proteins. F indicates the position of the Mlph-interacting motif encoded by alternatively spliced exon F. (B) Representative images showing the distribution of each GFP fusion and melanosomes (bright-field) in melanocytes (scale bar = 20 μm). (C, D) Scatter plots showing the melanosome dispersion (C) and circularity (D) of individual melanocytes expressing the indicated proteins. Horizontal bars show the median and 25th and 75th percentile of the each population. ****Significance of differences in populations of data (p = <0.0001) as determined by one-way analysis of variance. No other significant differences were observed. Data are from one of three independent experiments and are representative of the results of all experiments. Number of cells analyzed; GFP = 14, MyoVa = 25, Myo-Rab = 26, Myo-Mlph = 20. (E) Model indicating how the different arrangement of motors in Myo-Rab versus Myo-FL/Myo-Mlph might result in differences in dendrite formation.

Perturbation of dynamic interaction with melanosomes reduces the functional efficiency of MyoVa in transport and melanocyte dendrite formation

To test the functional importance of the dynamic association of MyoVa with melanosomes, we generated a vector that expresses a fusion protein (Myo-Rab) that can more stably target active MyoVa to melanosomes. This protein comprises a constitutively active, dimer-forming HMM (heavy meromyosin) fragment of MyoVa (i.e., containing the motor, lever, and dimerization domains, but lacking the melanosome-binding tail) fused to the N-terminus of the melanosome-targeted Rab27a^{SF1F4} mutant (Tarafder *et al.*, 2011) (Figure 5A). We then compared the rescue of melanosome transport defects in myosin-Va null (melan-d) cells (a readout of MyoVa function) expressing Myo-Rab and wild-type MyoVa.

Using confocal microscopy, we observed that Myo-Rab localized to, and dispersed melanosomes to, a significantly greater extent than GFP alone, but to a somewhat lesser extent (not significant) than Myo-FL (Figure 5, B and C [arrows in B highlight motor:melanosome association]; mean pigment area [% total]; Myo-FL = 80.64 ± 9.104, Myo-Rab = 75.52 ± 10.83, GFP = 21.04 ± 3.37). We also noted that Myo-Rab accumulated strongly in the F-actin–rich periphery of melanocytes (i.e., beyond the melanosome-filled area; Figure 5B, box 2) and that cells expressing this fusion were significantly less elongated and more rounded than those expressing GFP-MyoVa (Figure 5, B and D; circularity [arbitrary units; AU]; Myo-FL = 0.24 ± 0.085, Myo-Rab = 0.57 ± 0.16, GFP = 0.25 ± 0.11). Observation of F-actin distribution did not reveal striking differences among cells expressing the different MyoVa proteins (Figure 5). Quantitative analysis of F-actin and MyoVa distribution in melan-d cells in which x/y cell shape was normalized by culture on disk-shaped micropatterns confirmed that F-actin distribution is similar in Myo-FL– and Myo-Rab–expressing cells and the peripheral accumulation of Myo-Rab (Supplemental Figure S5) (Evans *et al.*, 2014). Expression of Myo-Rab in Rab27a- and Mlph-deficient melanocytes gave similar results, suggesting that dynamic interaction with cargo enhances MyoVa function in melanosome dispersion and dendrite development (Supplemental Figure S6).

An alternative (or additional) mechanistic basis for these observations is that the function of Myo-Rab is compromised by the

constitutive activity of its MyoVa component, a consequence of the replacement of the Myo-T with Rab27a^{SF1F4} in this chimera. Previous studies have shown that, in the absence of cargo, Myo-T may interact with and inhibit the motor/ATPase "head" domain of MyoVa, and in yeast this regulatory interaction is important for type V myosin (Myo2) function in organelle inheritance (Krementsov *et al.*, 2004; Li *et al.*, 2004; Wang *et al.*, 2004; Donovan and Bretscher, 2015). To determine the extent that loss of MyoVa head–tail regulation contributes to the difference in function of Myo-Rab versus Myo-FL, we generated another active myosin fusion protein, Myo-Mlph, in which the Rab27a^{SF1F4} portion of Myo-Rab was replaced with the R27BD of Mlph (Figure 5A). smFRAP studies revealed that Mlph-R27BD alone turns over rapidly on melanosomes like wild-type Mlph (Supplemental Figure S6 and Supplemental Movie 14). Thus, the Myo-Mlph allows active dimeric MyoVa to dynamically associate with melanosomes via interaction with endogenous Rab27a. When expressed in myosin-Va –/– (melan-d) cells, we found that Myo-Mlph localized to and dispersed melanosomes to a similar extent to Myo-Rab, but did not affect the dendrite development (Figure 5, B–D; mean pigment area [% total] = 75.61 ± 10.29; circularity [AU] = 0.23 ± 0.069). Using smFRAP, we confirmed that Myo-Rab associated with melanosomes stably similar to Rab27a (mean maximum recovery [% total] = 31 ± 8.715) (Supplemental Figure S7 and Supplemental Movie 15). These observations suggest that regulation of MyoVa, although not essential, is important for optimal function in melanosome dispersion and that dynamic MyoVa:melanosomes association is important for dendrite development.

DISCUSSION

Here we investigated how adaptor proteins regulate motor:cargo interactions and transport using as a model melanosomes (cargo) in melanocytes, MyoVa (motor), and Rab27a and Mlph (cargo adaptors). Our novel findings are fourfold.

First, using smFRAP, we discovered that MyoVa dynamically associates with melanosomes in mouse melanocytes (Figure 1). To our knowledge, no previous study has investigated the kinetics of association of MyoVa with cargo in mammalian cells. In fission yeast FRAP revealed that type V myosin (myo51) turned over rapidly ($t_{1/2}$ = 6.7 ± 1.4 s) at the contractile ring during cytokinesis (Wang *et al.*, 2014). FRAP studies in HeLa cells revealed that myosin-VI turned over rapidly on endosomes ($t_{1/2}$ ~ 15 s) (Bond *et al.*, 2012). With our data, this suggests that rapid turnover at sites of action may be a conserved facet of nonmuscle myosins. However, whereas endosomes and contractile rings are short-lived structures that might be expected to rapidly exchange their contents and distribution as part of their function, melanosomes are not. Melanosome biogenesis takes several days in vitro and mature melanosomes can persist in cells for several days (Sviderskaya *et al.*, 1995; Wasmeier *et al.*, 2006). This suggests that MyoVa-dependent melanosome dispersion is likely to be composed of multiple short episodes of Mlph/MyoVa:melanosome interactions and movements that guide melanosomes collectively toward, and into, peripheral dendrites.

Second, we found that dynamic Mlph:Rab27a interaction, and not Rab27a:melanosome interaction, is the dominant factor regulating dynamic MyoVa:melanosome interaction. These findings are consistent with FRAP data showing low turnover of Rab27a on secretory granules in PC12 cells, human umbilical vein epithelium cells (HUVECs), and melanocytes and higher turnover of effector Rabphilin in PC12 cells (recovery Rab27a = 37.8% [PC12], none detected [HUVEC], 15% [melanocyte]; Rabphilin-3a = 66%, $t_{1/2}$ = 15.4 s) (Jordens *et al.*, 2006; Handley *et al.*, 2007; Handley and Burgoyne, 2008; Kiskin *et al.*, 2010). Our results also agree with non-FRAP studies showing 1) low affinity of Mlph:Rab27a interaction relative to other effectors (K_d = 112 nM [Mlph] vs. 13.4 nM [Sytl2-a]), 2) relatively low intrinsic GTPase activity (~30-fold lower than Rab5a) of Rab27a in vitro, and 3) stable membrane association of GDP-bound Rab27a in platelets (Larijani *et al.*, 2003; Fukuda, 2006; Kondo *et al.*, 2006). Overall, these data suggest that Rab27a in melanocytes (like platelets) is mainly GTP-bound and that, in some cases, Rab-GTP:effector interaction stability governs effector recruitment to membranes rather than GTP/GDP status and membrane/cytosol cycling of Rab, as proposed by general models of Rab function (Stenmark, 2009; Hutagalung and Novick, 2011; Pfeffer, 2017). Consistent with this, smFRAP studies revealed that the R27BD of the high-affinity effector Sytl2-a turned over to a significantly lower extent than Mlph on melanosome membranes (Supplemental Figures S2 and S8 and Supplemental Movie 16; mean maximum recovery [%PBFI] = 30.34% ± 11.13%). Unfortunately, we were unable to use smFRAP to confirm the GTP/GDP status of Rab27a, as we found that GTP-/GDP-locked Rab27a mutants (Q78L and T23N) did not obviously associate with melanosomes (Supplemental Figure S9).Other studies have reported similar findings (Hume *et al.*, 2001; Bahadoran *et al.*, 2003; Ishida *et al.*, 2014).

Third, we discovered that disruption of head–tail regulation of MyoVa in melanocytes (as in Myo-Rab and Myo-Mlph) partially reduced its efficiency in melanosome dispersion and resulted in the accumulation of the protein in the peripheral cytoplasm (Figure 5; Supplemental Figure S5). This is consistent with data from yeast showing that disruption of head–tail regulation of the type V myosin Myo2 caused defects in organelle inheritance, accumulation of Myo2 in the daughter bud tip, and reduced proliferation (Donovan and Bretscher, 2015). A possible mechanistic explanation for the reduced function of Myo-Rab and Myo-Mlph is that in Myo-FL, the head–tail regulation ensures that motors are only active when associated with cargo. Thus, when the Myo-FL and cargo uncouple, then Myo-FL inactivates, detaches from F-actin, and may be recycled for further rounds of transport. On the other hand, active MyoVa (Myo-Rab and Myo-Mlph) can move toward the +/barbed ends of F-actin and remain there even without cargo. Consistent with this, both active MyoVa fusions tested here (Myo-Rab and Myo-Mlph) accumulated in the peripheral cytoplasm, a region of melanocytes previously found to be enriched in F-actin–rich, filopod-like structures and active MyoVa proteins (Kapitein *et al.*, 2013; Robinson *et al.*, 2017). It is likely that this peripheral accumulation reduces the efficiency of initial MyoVa:melanosome association, bearing in mind that melanosomes in MyoVa-deficient cells accumulate in the perinuclear cytoplasm and also precludes MyoVa recycling.

Fourth, we found that dynamic MyoVa:melanosome interaction is required for the development of elongated, pigment-filled dendrites. Dendrites are a hallmark of melanocytes and are thought to be the prime sites of melanosome transfer to keratinocytes. Specifically, we observed that expression of Myo-Rab in MyoVa –/– (melan-d) cells significantly increased cell roundness compared with Myo-Mlph and Myo-FL. One possible explanation for this may lie in the observation that Myo-Rab (and Rab27a) appears more uniformly distributed over the surface of melanosomes, compared with Myo-Mlph (and Mlph/MyoVa), which often localize in spots adjacent to melanosomes (Supplemental Figure S3C; Figure 5B). We suggest that spots or clusters of Mlph/MyoVa might allow coordination of the activity of individual motors and directed movement of melanosomes along F-actin bundles toward dendrite tips by ensuring that melanosomes remain associated with local F-actin bundles for longer than those where motors act alone. In contrast, the uniformly distributed Myo-Rab might allow melanosomes to engage a larger number of more randomly

oriented F-actin for shorter durations, thereby undertaking less directed transport (Figure 5E). Consistent with this, recent single molecule studies have revealed that small teams of myosin-Vc can more efficiently transport cargo along F-actin bundles compared with individual motors on individual filaments(Krementsova *et al.*, 2017). Related to this, it is possible that clustering of Mlph/MyoVa might also facilitate the clustering of F-actin and the formation of filament bundles. Supportive of this, the C-terminus of Mlph can interact with actin and expression of active dimeric MyoVa can bundle F-actin during the formation of filopodia-like structures in culture (Kuroda *et al.*, 2003; Kapitein *et al.*, 2013; Robinson *et al.*, 2017). Alternatively, other Mlph/MyoVa-tail interacting proteins, for example, end-binding protein 1, might contribute to dendrite development by allowing interaction with cytoskeleton elements such as microtubules and intermediate filaments that are present in melanocyte dendrites (Wu *et al.*, 2005; Hume *et al.*, 2007). A further possibility is that a nonmelanosomal pool of Mlph/MyoVa, or interacting partners, contributes to dendrite development. Thus, in Myo-Rab–expressing cells, the activity of the nonmelanosomal pool would be altered, thereby reducing dendrites development.

Finally, our finding that Myo-Rab can rescue melanosome dispersion in vitro with relatively high efficiency is surprising, given the differences in turnover of this protein compared with Myo-FL and the loss of the contribution of Mlph and potentially other interacting proteins. Given the importance of dendrites in melanosome transfer from melanocytes to keratinocytes, we suggest that our results using melanosome dispersion after transient overexpression of MyoVa proteins to measure function may underestimate the in vivo significance of dynamic turnover of MyoVa. In vivo protein expression levels are likely to be lower than here, meaning that recycling is more important for MyoVa function, and the formation of dendrites is critical for the transfer of pigment to keratinocytes. Consistent with this, expression of physiological levels of head–tail mutants by modification of the *MYO2* gene in yeast resulted in strong reductions in proliferation (Donovan and Bretscher, 2015).

MATERIALS AND METHODS

Plasmid and virus constructs

pEGFPC3-Rab27a, pEGFPC3-Rab27a^{SF1F4}, pEGFPC3-Mlph, and pEGFPC3-MyoVa-tail (MSGTA—here Myo-T encoding amino acids 1277–1877 of the murine MyoVa encoded by transcript XM_006510828.1) were previously described (Hume *et al.*, 2001; Strom *et al.*, 2002; Tarafder *et al.*, 2011). pENTRmCherryC2-Mlph was made by subcloning the full murine Mlph coding sequence from pEGFPC3-Mlph into pENTRmCherryC2 supplied by Jose Ramalho (Nova Universidad de Lisboa, Lisboa, Portugal). pENTRmCherryC2-MlphΔRBD-Rab27a^{SF1F4} encoding a fusion protein comprising from the N-terminus of mCherry, the C-terminus MyoVa- and actin-binding domains (and lacking the N-terminus Rab27a-binding domain) fused to the N-terminus of melanosome targeted, but nonfunctional, Rab27a^{SF1F4} mutant, was generated by sequential subcloning of the coding sequence for MlphΔRBD (amino acids 150–590 of murine Mlph; NM_053015) and Rab27a^{SF1F4} into pENTRmCherryC2. pENTR-GFPC2-MyoVa (HMM)-Rab27a^{SF1F4} was generated using a similar sequential subcloning approach (MyoVa [HMM] corresponds to the sequence coding the XM_006510828.1 motor, lever, and dimerization domains of MyoVa heavy chain but lacking the melanocyte-specific, Mlph-binding exons D and F and cargo-binding tail [amino acids 1–1300 of the murine protein; XM_006510828.1]). The generation of adenoviruses allowing expression of the GFP alone, GFP-MyoVa, and GFP-MyoVa (HMM)-Rab27a^{SF1F4} in melanocytes was as previously described (Hume *et al.*, 2006).

Cell culture and transfection

Cultures of immortal melan-a (wild-type), melan-d1 (myosin-Va null), melan-ln (Mlph null), and melan-ash (Rab27a null) melanocytes were maintained in RPMI 1640 medium supplemented with 10% fetal calf serum (FCS), 2 mM glutamine, 100 U/ml penicillin G, 100 mg/ml streptomycin, and 200 nM phorbol 12-myristate 13-acetate (all Sigma-Aldrich, Poole, United Kingdom) at 37°C with 10% CO_2 as described previously (Evans *et al.*, 2014). For live cell experiments and functional studies, cells were plated onto 35-mm-diameter glass-bottomed Petri dishes (Matek P35G-1.5–20-C) (5×10^4 cells/dish) and 13-mm glass coverslips (1×10^4 cells/coverslip), respectively, and the next day transfected with plasmids or infected with adenovirus, allowing expression of EGFP fusion proteins. Transfection was carried out using Fugene 6 (Promega, UK) as previously described (Hume *et al.*, 2006) and cells were imaged fixed or alive 48 h later. For live cell experiments, growth medium was replaced with L-15 medium supplemented with 10% FCS, 100 U/ml penicillin G, and 100 mg/ml streptomycin.

Fluorescence microscopy

Cells for immunofluorescence were paraformaldehyde fixed and stained and fluorescence and bright-field images showing GFP fusion protein and melanosome distribution, respectively. Images were captured using Axiovision 4.8 software associated with a Zeiss Axiovert 100S inverted microscope fitted with a 40 × 1.4NA oil immersion Apochromat objective lens and an Axiocam MR-3 CCD camera, as previously described (Robinson *et al.*, 2017). Antibodies used were mouse monoclonal anti-GFP (Roche 11814460001; 1:300) and goat anti-mouse immunoglobulin G (H+L) cross-adsorbed secondary antibody, Alexa Fluor 568-labeled (Molecular Probes A-11004; 1:500).

For live cell/smFRAP experiments, after medium change, cells were transferred to the stage of a Zeiss LSM710 confocal microscope fitted with a 63 × 1.4NA oil immersion Apochromat lens within an environmental chamber (37°C). Cells were imaged using a 488-nm argon and 561-nm HeNe lasers to visualize GFP and mCherry, respectively, and melanosomes were imaged using transmitted light simultaneously with GFP. All images presented here are single sections in the *z*-plane. For FRAP sequences, images were acquired every 1.56 s (for GFP-Rab27a) or 1.94 s (for GFP-Mlph and Myo-T). EGFP fusion proteins were excited using a 488-nm argon laser set to 2% power with pinhole set to 1 airy unit. To facilitate downstream FRAP analysis, circular bleach regions were defined around single melanosomes well separated from other organelles in thin, flat areas of melanocyte cytoplasm in cells that exhibited high signal:noise ratio (melanosome-associated:cytosolic fluorescent protein) and, where appropriate, in cells in which EGFP expression restored dispersed melanosome distribution (indicating physiologically relevant levels of expression). Bleaching of GFP was carried out by scanning these regions five times using the 488-nm laser at 100%. For each FRAP series, five images were acquired prior to bleaching to establish the 100% level of fluorescence signal associated with each melanosome and then up to 200 images were acquired after bleaching to monitor recovery of melanosome-associated fluorescence.

Image analysis

To determine the rate of fluorescence recovery in bleached melanosomes, image sequences were exported from Zen 2011 software and imported to Volocity 6 image analysis software (Improvision) that allows automatic particle tracking. Melanosomes visible in transmitted light images were defined using intensity and size/area

filters and then tracked using the shortest path-tracking model within Volocity 6, and EGFP signal associated with individual melanosomes over time was extracted as previously described (Hume *et al.*, 2011). Signal associated with bleached melanosomes was then normalized by comparison with nonbleached melanosomes in the same cell and converted to percentage of maximum/prebleach signal. To determine the extent (plateau) and kinetics ($t_{1/2}$) of the fluorescence recovery experiment using Mlph and MyoT, postbleach data were imported into GraphPad Prism 7 software and each record was fitted to a single exponential function using the nonlinear regression curve fit facility. For all data, the maximum fluorescence recovery was determined using Graphpad Prism 7 software. Measurement of the function of experimental MyoVa fusion proteins in melanosome transport (Figure 5) was based on manual measurement of the proportion of cell area occupied by pigmented melanosomes as previously described (Hume *et al.*, 2006). Cell circularity was determined using the formula $4\Pi A/P^2$; where A = cell area and P = cell perimeter.

ACKNOWLEDGMENTS

We thank Tim Self (confocal microscopy), Sue Cooper, and Carol Sculthorpe (general) (all University of Nottingham, UK) for technical assistance. This work was supported by a Medical Research Council New Investigator Award to A.N.H. (Grant G1100063) and a Biotechnology and Biological Sciences Research Council grant (BB/F016956/1) and University of Nottingham–funded PhD studentship awarded to C.L.R.

REFERENCES

Bahadoran P, Aberdam E, Mantoux F, Busca R, Bille K, Yalman N, De Saint-Basile G, Casaroli-Marano R, Ortonne JP, Ballotti R (2001). Rab27a: a key to melanosome transport in human melanocytes. J Cell Biol 152, 843–850.

Bahadoran P, Busca R, Chiaverini C, Westbroek W, Lambert J, Bille K, Valony G, Fukuda M, Naeyaert JM, Ortonne JP, Ballotti R (2003). Characterization of the molecular defects in Rab27a, caused by RAB27A missense mutations found in patients with Griscelli syndrome. J Biol Chem 278, 11386–11392.

Barr FA (2013). Review series: Rab GTPases and membrane identity: causal or inconsequential? J Cell Biol 202, 191–199.

Bond LM, Arden SD, Kendrick-Jones J, Buss F, Sellers JR (2012). Dynamic exchange of myosin VI on endocytic structures. J Biol Chem 287, 38637–38646.

Chernyakov I, Santiago-Tirado F, Bretscher A (2013). Active segregation of yeast mitochondria by Myo2 is essential and mediated by Mmr1 and Ypt11. Curr Biol 23, 1818–1824.

Donovan KW, Bretscher A (2015). Head-to-tail regulation is critical for the in vivo function of myosin V. J Cell Biol 209, 359–365.

Evans RD, Robinson C, Briggs DA, Tooth DJ, Ramalho JS, Cantero M, Montoliu L, Patel S, Sviderskaya EV, Hume AN (2014). Myosin-Va and dynamic actin oppose microtubules to drive long-range organelle transport. Curr Biol 24, 1743–1750.

Fukuda M (2006). Distinct Rab27A binding affinities of Slp2-a and Slac2-a/melanophilin: hierarchy of Rab27A effectors. Biochem Biophys Res Commun 343, 666–674.

Fukuda M (2013). Rab27 effectors, pleiotropic regulators in secretory pathways. Traffic 14, 949–963.

Fukuda M, Kuroda TS, Mikoshiba K (2002). Slac2-a/melanophilin, the missing link between Rab27 and myosin Va: implications of a tripartite protein complex for melanosome transport. J Biol Chem 277, 12432–12436.

Hammer JA 3rd, Sellers JR (2012). Walking to work: roles for class V myosins as cargo transporters. Nat Rev Mol Cell Biol 13, 13–26.

Hammer JA 3rd, Wu XS (2002). Rabs grab motors: defining the connections between Rab GTPases and motor proteins. Curr Opin Cell Biol 14, 69–75.

Handley MT, Burgoyne RD (2008). The Rab27 effector Rabphilin, unlike Granuphilin and Noc2, rapidly exchanges between secretory granules and cytosol in PC12 cells. Biochem Biophys Res Commun 373, 275–281.

Handley MT, Haynes LP, Burgoyne RD (2007). Differential dynamics of Rab3A and Rab27A on secretory granules. J Cell Sci 120, 973–984.

Hartman MA, Finan D, Sivaramakrishnan S, Spudich JA (2011). Principles of unconventional myosin function and targeting. Annu Rev Cell Dev Biol 27, 133–155.

Hirokawa N, Noda Y, Tanaka Y, Niwa S (2009). Kinesin superfamily motor proteins and intracellular transport. Nat Rev Mol Cell Biol 10, 682–696.

Hume AN, Collinson LM, Rapak A, Gomes AQ, Hopkins CR, Seabra MC (2001). Rab27a regulates the peripheral distribution of melanosomes in melanocytes. J Cell Biol 152, 795–808.

Hume AN, Seabra MC (2011). Melanosomes on the move: a model to understand organelle dynamics. Biochem Soc Trans 39, 1191–1196.

Hume AN, Tarafder AK, Ramalho JS, Sviderskaya EV, Seabra MC (2006). A coiled-coil domain of melanophilin is essential for Myosin Va recruitment and melanosome transport in melanocytes. Mol Biol Cell 17, 4720–4735.

Hume AN, Ushakov DS, Tarafder AK, Ferenczi MA, Seabra MC (2007). Rab27a and MyoVa are the primary Mlph interactors regulating melanosome transport in melanocytes. J Cell Sci 120, 3111–3122.

Hume AN, Wilson MS, Ushakov DS, Ferenczi MA, Seabra MC (2011). Semi-automated analysis of organelle movement and membrane content: understanding rab-motor complex transport function. Traffic 12, 1686–1701.

Hutagalung AH, Novick PJ (2011). Role of Rab GTPases in membrane traffic and cell physiology. Physiol Rev 91, 119–149.

Ishida M, Arai SP, Ohbayashi N, Fukuda M (2014). The GTPase-deficient Rab27A(Q78L) mutant inhibits melanosome transport in melanocytes through trapping of Rab27A effector protein Slac2-a/melanophilin in their cytosol: development of a novel melanosome-targetinG tag. J Biol Chem 289, 11059–11067.

Jordens I, Westbroek W, Marsman M, Rocha N, Mommaas M, Huizing M, Lambert J, Naeyaert JM, Neefjes J (2006). Rab7 and Rab27a control two motor protein activities involved in melanosomal transport. Pigment Cell Res 19, 412–423.

Kapitein LC, Van Bergeijk P, Lipka J, Keijzer N, Wulf PS, Katrukha EA, Akhmanova A, Hoogenraad CC (2013). Myosin-V opposes microtubule-based cargo transport and drives directional motility on cortical actin. Curr Biol 23, 828–834.

Kardon JR, Vale RD (2009). Regulators of the cytoplasmic dynein motor. Nat Rev Mol Cell Biol 10, 854–865.

Kiskin NI, Hellen N, Babich V, Hewlett L, Knipe L, Hannah MJ, Carter T (2010). Protein mobilities and P-selectin storage in Weibel-Palade bodies. J Cell Sci 123, 2964–2975.

Kondo H, Shirakawa R, Higashi T, Kawato M, Fukuda M, Kita T, Horiuchi H (2006). Constitutive GDP/GTP exchange and secretion-dependent GTP hydrolysis activity for Rab27 in platelets. J Biol Chem 281, 28657–28665.

Krementsov DN, Krementsova EB, Trybus KM (2004). Myosin V: regulation by calcium, calmodulin, and the tail domain. J Cell Biol 164, 877–886.

Krementsova EB, Furuta K, Oiwa K, Trybus KM, Ali MY (2017). Small teams of myosin Vc motors coordinate their stepping for efficient cargo transport on actin bundles. J Biol Chem 292, 10998–11008.

Kuroda TS, Ariga H, Fukuda M (2003). The actin-binding domain of Slac2-a/melanophilin is required for melanosome distribution in melanocytes. Mol Cell Biol 23, 5245–5255.

Larijani B, Hume AN, Tarafder AK, Seabra MC (2003). Multiple factors contribute to inefficient prenylation of Rab27a in Rab prenylation diseases. J Biol Chem 278, 46798–46804.

Li XD, Mabuchi K, Ikebe R, Ikebe M (2004). Ca2+-induced activation of ATPase activity of myosin Va is accompanied with a large conformational change. Biochem Biophys Res Commun 315, 538–545.

Lindsay AJ, Jollivet F, Horgan CP, Khan AR, Raposo G, Mccaffrey MW, Goud B (2013). Identification and characterization of multiple novel Rab-myosin Va interactions. Mol Biol Cell 24, 3420–3434.

Lipatova Z, Tokarev AA, Jin Y, Mulholland J, Weisman LS, Segev N (2008). Direct interaction between a myosin V motor and the Rab GTPases Ypt31/32 is required for polarized secretion. Mol Biol Cell 19, 4177–4187.

Nagashima K, Torii S, Yi Z, Igarashi M, Okamoto K, Takeuchi T, Izumi T (2002). Melanophilin directly links Rab27a and myosin Va through its distinct coiled-coil regions. FEBS Lett 517, 233–238.

Pfeffer SR (2017). Rab GTPases: master regulators that establish the secretory and endocytic pathways. Mol Biol Cell 28, 712–715.

Robinson CL, Evans RD, Briggs DA, Ramalho JS, Hume AN (2017). Inefficient recruitment of kinesin-1 to melanosomes precludes it from facilitating their transport. J Cell Sci 130, 2056–2065.

Stenmark H (2009). Rab GTPases as coordinators of vesicle traffic. Nat Rev Mol Cell Biol 10, 513–525.
Strom M, Hume AN, Tarafder AK, Barkagianni E, Seabra MC (2002). A family of Rab27-binding proteins. Melanophilin links Rab27a and myosin Va function in melanosome transport. J Biol Chem 277, 25423–25430.
Sviderskaya EV, Wakeling WF, Bennett DC (1995). A cloned, immortal line of murine melanoblasts inducible to differentiate to melanocytes. Development 121, 1547–1557.
Tarafder AK, Wasmeier C, Figueiredo AC, Booth AE, Orihara A, Ramalho JS, Hume AN, Seabra MC (2011). Rab27a targeting to melanosomes requires nucleotide exchange but not effector binding. Traffic 12, 1056–1066.
Trybus KM (2008). Myosin V from head to tail. Cell Mol Life Sci 65, 1378–1389.
Van Den Bossche K, Naeyaert JM, Lambert J (2006). The quest for the mechanism of melanin transfer. Traffic 7, 769–778.
Van Gele M, Dynoodt P, Lambert J (2009). Griscelli syndrome: a model system to study vesicular trafficking. Pigment Cell Melanoma Res 22, 268–282.
Wang F, Thirumurugan K, Stafford WF, Hammer JA 3rd, Knight PJ, Sellers JR (2004). Regulated conformation of myosin V. J Biol Chem 279, 2333–2336.
Wang Z, Edwards JG, Riley N, Provance DW Jr, Karcher R, Li XD, Davison IG, Ikebe M, Mercer JA, Kauer JA, Ehlers MD (2008). Myosin Vb mobilizes recycling endosomes and AMPA receptors for postsynaptic plasticity. Cell 135, 535–548.
Wang N, Lo Presti L, Zhu YH, Kang M, Wu Z, Martin SG, Wu JQ (2014). The novel proteins Rng8 and Rng9 regulate the myosin-V Myo51 during fission yeast cytokinesis. J Cell Biol 205, 357–375.
Wasmeier C, Romao M, Plowright L, Bennett DC, Raposo G, Seabra MC (2006). Rab38 and Rab32 control post-Golgi trafficking of melanogenic enzymes. J Cell Biol 175, 271–281.
Wu X, Bowers B, Rao K, Wei Q, Hammer JA 3rd (1998). Visualization of melanosome dynamics within wild-type and dilute melanocytes suggests a paradigm for myosin V function In vivo. J Cell Biol 143, 1899–1918.
Wu X, Hammer JA (2014). Melanosome transfer: it is best to give and receive. Curr Opin Cell Biol 29, 1–7.
Wu X, Rao K, Bowers MB, Copeland NG, Jenkins NA, Hammer JA 3rd (2001). Rab27a enables myosin Va-dependent melanosome capture by recruiting the myosin to the organelle. J Cell Sci 114, 1091–1100.
Wu X, Wang F, Rao K, Sellers JR, Hammer JA 3rd (2002a). Rab27a is an essential component of melanosome receptor for myosin Va. Mol Biol Cell 13, 1735–1749.
Wu XS, Rao K, Zhang H, Wang F, Sellers JR, Matesic LE, Copeland NG, Jenkins NA, Hammer JA 3rd (2002b). Identification of an organelle receptor for myosin-Va. Nat Cell Biol 4, 271–278.
Wu XS, Tsan GL, Hammer JA 3rd (2005). Melanophilin and myosin Va track the microtubule plus end on EB1. J Cell Biol 171, 201–207.